

Practical polarization maintaining optical fibre temperature sensor for harsh environment application

This content has been downloaded from IOPscience. Please scroll down to see the full text.

2007 Meas. Sci. Technol. 18 3235

(<http://iopscience.iop.org/0957-0233/18/10/S28>)

View [the table of contents for this issue](#), or go to the [journal homepage](#) for more

Download details:

IP Address: 222.195.76.141

This content was downloaded on 26/03/2015 at 03:03

Please note that [terms and conditions apply](#).

Practical polarization maintaining optical fibre temperature sensor for harsh environment application

Yuanhong Yang¹, Haiyun Xia¹ and Wei Jin²

¹ The Institute of Optoelectronics Technology, BeiHang University, Beijing, People's Republic of China

² Department of Electrical Engineering, The Hong Kong Polytechnic University, Hong Kong

Received 2 January 2007, in final form 28 March 2007

Published 12 September 2007

Online at stacks.iop.org/MST/18/3235

Abstract

A reflection spot temperature sensor was proposed based on the polarization mode interference in polarization maintaining optical fibre (PMF) and the phenomenon that the propagation constant difference of the two orthogonal polarization modes in stressing structures PMF is sensitive to temperature and the sensing equation was obtained. In this temperature sensor, a broadband source was used to suppress the drift due to polarization coupling in lead-in/lead-out PMF. A characteristic and performance investigation proved this sensor to be practical, flexible and precise. Experimental results fitted the theory model very well and the noise-limited minimum detectable temperature variation is less than 0.01 °C. The electric arc processing was investigated and the differential propagation constant modifying the PMF probe is performed. For the demand of field hot-spot monitoring of huge power transformers, a remote multi-channel temperature sensor prototype has been made and tested. Specially coated Panda PMF that can stand high temperatures up to 250 °C was fabricated and used as probe fibres. The sensor probes were sealed within thin quartz tubes that have high voltage insulation and can work in a hot oil and vapour environment. Test results show that the accuracy of the system is better than ± 0.5 °C within 0 °C to 200 °C.

Keywords: spot temperature sensor, polarization maintaining fibre, hotspot field monitoring, power transformers

(Some figures in this article are in colour only in the electronic version)

1. Introduction

Optical fibre can be used to measure a number of physical parameters such as temperature and strain [1–3]. Compared with their electric counterparts, fibre optic sensors are made from dielectric materials and hence are well suited for measurement and condition monitoring in the power industry because power generation, transformation and distribution are in general carried out in harsh (high radiation, humidity, vibrations, high voltage etc) environments. A number of research groups have developed fibre sensors for the power industry and have successfully conducted field trials [4–6].

For the purpose of design verification, lifetime calculation and full dynamic loading management, transformer hot spot measurement systems have been developed and used successfully by LUXTRON Corporation with non-conductive and non-metallic fluoroptic temperature sensor technology [7]. The measurement accuracy of the system is ± 2 °C within -30 °C to 200 °C. Recently, we proposed a precision temperature sensor technology with a Sagnac-like interferometer [8, 9]. Based on this technology, an alternative temperature sensor scheme is proposed and a multi-channel temperature sensor for field hot-spot monitoring in power transformers is developed in this paper, and good performance has been achieved.

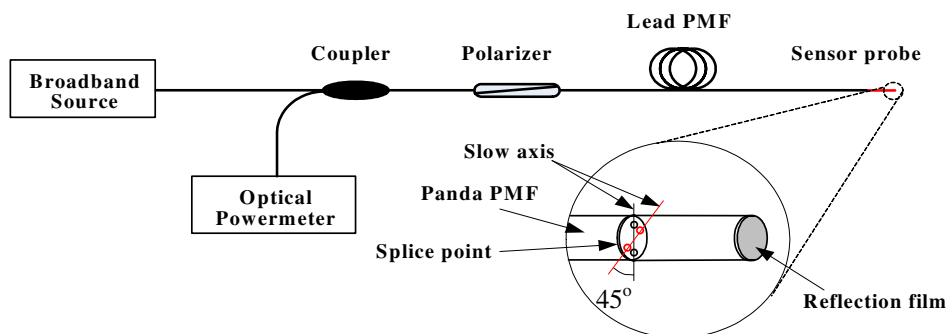


Figure 1. Schematic diagram of the temperature sensor.

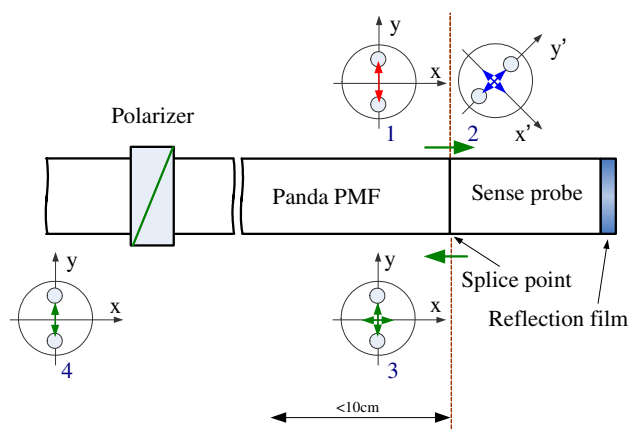


Figure 2. The polarization mode coupling process along the optical path.

2. Principle of operation

Figure 1 shows a schematic of the spot temperature sensor. The sensor is comprised of a broadband source, a 2×2 coupler, a high extinction ratio polished PMF polarizer and lead-in/lead-out PMF for connecting the polarizer and sensing probe. The sensing probe is a short section of PMF with its principal axes aligned with 45° offset with respect to the rest of the PMFs (see the inset in figure 1). A highly reflective dielectric film is deposited on the far end of the sensing probe to form a mirror. Along the optical path, the polarization mode coupling process is shown in figure 2, where y denotes the slow axis, x denotes the fast axis and the arrow line denotes the polarization mode. The broadband light is polarized after passing through the coupler and polarizer and propagates along the lead-in/lead-out PMF, as shown in section 1 in figure 2. At the splice point, as shown in section 2 in figure 2, two orthogonal polarization eigenmodes will be excited and propagated in the PMF sensor probe because of the 45° angle offset at this point. The reflected light will go backward along the same path. When they pass the splice point again, each polarization mode will excite two other orthogonal polarization modes in the PMF too, as shown in section 3 in figure 2. Then four polarization modes with different phase information, namely $yy'x$, $yy'y$, $yx'x$, $yx'y$, propagate in the lead PMF. When they reach the polarizer, only the components with polarization orientation parallel to the polarizer, namely $yy'y$ and $yx'y$,

can pass and reach the powermeter, as shown in section 4 in figure 2. Their phase difference is

$$\delta = 2 \cdot \Delta\beta \cdot L \tag{1}$$

where $\Delta\beta$ is the difference between the propagation constants of the two orthogonal polarization states, L is the length of the sensing PMF probe and δ occurs only in the sensor PMF probe. They will interfere in PMF and the output interference signal may be described as [8, 9]

$$I = K \cdot (1 + \gamma(\delta) \cdot \cos \delta) \tag{2}$$

where K is a constant proportional to the power of the light source and $\gamma(\delta)$ is the coherence function of the broadband source. For PMFs, such as Panda- and bow-tie-type, made by adding additional stressing structures in the cladding, $\Delta\beta$ will decrease with increase in temperature within -200 – 400°C and the coefficient [10, 11] is about negative 10^{-3} magnitude. The PMF length change with temperature can be ignored because the coefficient is 10^{-6} magnitude. So, δ may be written as

$$\delta = a_0 + a_1 T \tag{3}$$

where a_1 , a_2 are coefficients and T is the temperature to be sensed.

In this sensor, the bandwidth of the broadband light source is about 30 nm. When it coupled on both modes of a high-birefringence fibre (as shown in section 2 in figure 2), there are at a certain position in PMF two wave trains which do not overlap if their path difference is larger than the decoherence length L_{dc} of this source; the light then becomes statistically depolarized. The length of fibre required to get such a depolarization is called the depolarization length L_d . The relationship between L_{dc} and L_d can be described as follows [12]:

$$\frac{L_d}{L_{dc}} = \frac{\Lambda}{\lambda} \tag{4}$$

where Λ is the beatlength of the PMF used and λ is the mean wavelength of the source. The beatlength of PMFs is within 1.5–4 mm, the wavelength is 1300 nm or 1550 nm; so the depolarization length is several centimetres. It means that the orthogonal polarization modes excited in the sensor probe can interfere only within a range of several centimetres from the probe PMF end. The polarization mode coupling intensity is very weak in the short PMF length (less than 10 cm, as shown in figure 2). So, the phase difference δ in the output

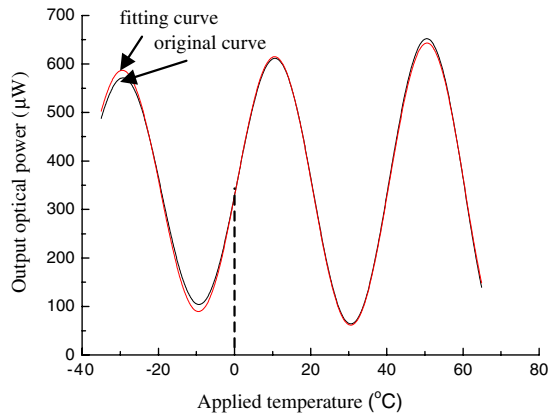


Figure 3. Experimental results and fitting curve.

interference signal (as described by equation (2)) occurs only in the sensor probe, and the other defect in lead-in/lead-out PMF will not induce error. This makes this temperature sensor practical.

From equations (1)–(3), it is obvious that the measurement range and sensitivity can be adjusted easily by changing the sensing PMF length.

3. Experimental study

To demonstrate the capability of the proposed sensor for precision temperature measurement, experiments were first carried out with a single sensor system, as shown in figure 1. A superluminescent diode (SLD) was taken as a broadband source and the mean wavelength is 1300 nm, the spectral width is about 30 nm, the lead-in/lead-out and sensing PMF were all Panda-type and the length of the sensing probe was arbitrarily chosen to be ~ 11.3 mm. The output optical power and the applied temperature were measured by a precision power meter and a precision thermometer and both sets of data were recorded continuously by a computer. Within the -45 °C– $+65$ °C temperature range, the curve of output power versus temperature is shown in figure 3 (the solid black line). The slow variation in the fringe contrast is due to the dependence of $\gamma(\delta)$ on temperature because of the short coherence length of the source. Because the reflectivity of the film at the end of the sensor, the exact length of the sensing probe, the beat length of the sensing PMF and the angle in orientation of the principal axes of the fibre and the feed fibre cannot be obtained accurately, the relationship between the sensor output and temperature can only be determined by calibration. To keep the fitting process simple, $\gamma(\delta)$ variation is assumed to be linear. According to equations (2) and (3), the curve shown in figure 3 may be fitted by the following equation:

$$V = (c_1 \cdot T + c_2) \cdot \cos(a_1 \cdot T + a_0) + c_3. \quad (5)$$

The fitting results are given in table 1, where c_1 represents the relation between $\gamma(\delta)$ and temperature, a_1 is the temperature coefficient of this sensor probe, c_2 , c_3 are bias values. The fitting curve is in figure 3 (red line) and fits the original measured curve very well. The error near peaks is due to the $\gamma(\delta)$ linear model error. It can be seen from figure 3 that the sensor output changed more than two cycles for

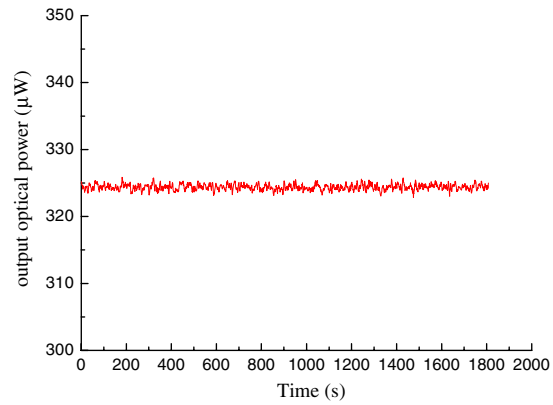


Figure 4. Sensor output at 0 °C.

Table 1. Fitting for $L = 11.3$ mm.

Parameter	c_1	c_2	a_1	a_0	c_3
Value	0.703	262.434	0.157	48.628	345.268

a temperature range from -45 °C– $+65$ °C. For effective measurement, however, the sensor output should have, within the entire measurement range, a monotonic relationship with temperature; hence the measurement range of this particular sensor ($L = 11.3$ mm) is limited to about 20 °C. To increase the measurement range, the sensing probe length should be shortened.

To evaluate the sensor performance in terms of noise-limited minimum detectable temperature variation, we submerge the sensor gauge in a mixture of ice and water, which provides a fixed temperature environment of 0 °C. As can be seen from figure 3, at this temperature the output signal level is about 324 μ W and the temperature sensitivity is near maximum with a slope coefficient of 46.71 μ W °C $^{-1}$. The output power is recorded for 30 min with a sample interval of 1 s. Figure 4 shows the measured results as a function of time. The standard derivation is 0.45 μ W over this 30 min period, corresponding to an equivalent temperature variation of 0.0096 °C.

4. Remote multi-channel temperature sensor

In a large power transformer, all possible hotspots must be monitored; hence a multi-channel system is necessary. In addition, the fibre section mounted within transformer oil needs to have high voltage insulation and to withstand high temperatures up to 200 °C and not react with the hot transformer oil.

4.1. Sensor configuration

Based on this sensing technology, a multi-channel sensor system was developed to monitor the hotspot temperature in the power transformer. The eight-channel temperature sensor system is shown in figure 5. An erbium doped fibre amplified spontaneous emission (EDF-ASE) source with 10 mW output power is used. The mean-wavelength of the source is 1545 nm and the FWHM bandwidth is 31 nm. The EDF-ASE source

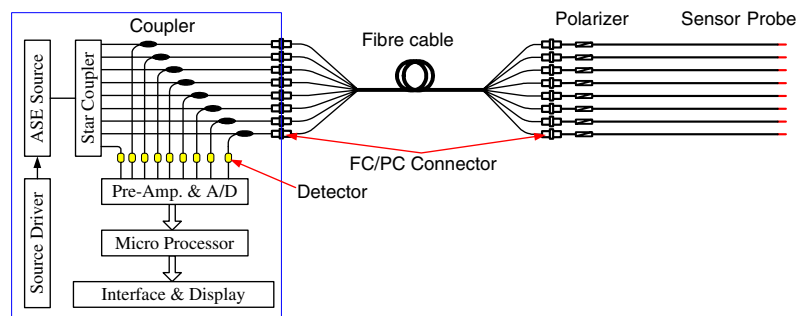


Figure 5. The eight-spot temperature sensor configuration.

has good mean-wavelength temperature stability and the temperature coefficient is better than $1.2 \text{ ppm } ^\circ\text{C}^{-1}$. A 1×9 star single-mode fibre coupler is used to split the source power into nine channels of approximately equal power. One of the channels is to monitor the source power variation and to use it as an intensity reference. The other eight channels correspond to eight temperature sensors with their operation principle shown in figure 1. As the output from the EDF-ASE source is polarization independent and the polarization dependent loss of the star coupler is also small, the degrees of light polarization in all eight channels are less than 0.02. The return light signals from the eight sensors are received by eight photo-detectors and the nine detector outputs are digitized through the use of an A/D converter. The micro-processor takes charge of procedure control and temperature calculation. The measured temperature values are sent to the interface and display module for display and to give analogue outputs, and RS-232 is designed to communicate with a computer, a 100 m signal mode fibre cable and the sensor section comprised of a polished PMF polarizer with extinction ratios greater than 28 dB and loss of less than 0.8 dB, the 2 m long lead-in/lead-out PMF and the 0.5 mm long sensor probe.

4.2. Sensor probe fabrication and packaging

In field applications, the lead-in/lead-out PMF and the sensor probe will be submerged in transformer oil; so a specially coated PMF which can withstand temperatures above 250°C is required. We have chosen panda PMF fibres with silica gel coating as the transmission and sensing PMF. The PMF has a beat length of 1.9 mm and a loss of 1.1 dB km^{-1} . The diameter of the coating is $250 \mu\text{m}$. To make sure that the output has a monotonic relationship with temperature over the measurement range of $0\text{--}200^\circ\text{C}$, the probe lengths of the eight sensors are chosen to be $\sim 0.5 \text{ mm}$.

Equation (2) indicates that there is a cosine relationship between the return power and the temperature. To make sure that the measurement is performed within the near linear range, the length of the PMF probe must be designed carefully. However, we found that it is very difficult to precisely control the probe length. To solve this problem, the electric arc processing of the PMF probe is taken to modify the differential propagation constant $\Delta\beta$, so the probe temperature response can be fine tuned. Figure 6 shows the experimental results obtained with a setup similar to that shown in figure 1 with a 1545 nm mean-wavelength broadband source and an about 1 mm length panda PMF probe. Curve 1 represents the

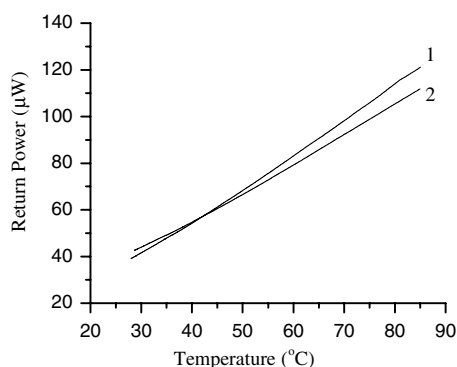


Figure 6. Sensor probe response change with electronic arc processing.

response without electric arc processing and curve 2 represents the response after twice processing with 6.5 mA and 1 s electric arc. The slope of the curve is changed from $1.97 \mu\text{W } ^\circ\text{C}^{-1}$ to $1.44 \mu\text{W } ^\circ\text{C}^{-1}$.

Figure 7 shows the sensor probe and packaging. Figure 7(a) shows eight sensors, each comprised of a FC connector, a PMF polarizer, 2 m lead-in/lead-out panda PMF and an about 0.5 mm long PMF sensor probe. The sensor probe is sealed within a thin quartz tube with the end fused as shown in figure 7(b). Figure 7(c) shows the bare sensor probe with $125 \mu\text{m}$ diameter and the reflection film deposited at the fibre end. The dielectric film made of SiO_2 and TiO_2 is deposited by using an electron beam coater and has excellent long-term stability and insulation. The transmission fibre and sensor probe are protected by the tube with $319 \mu\text{m}$ inner diameter and $436 \mu\text{m}$ outer diameter. The tube is coated with $20 \mu\text{m}$ thickness PMMA film. This ensures that the probe has high insulation and long-term durability in a harsh environment.

4.3. Linear modelling for sensor probe

In equation (5), there are five parameters needing to be calibrated or determined and the temperature calculation process is complicated. With careful selection of the sensor probe length and post electric arc processing, the sensor responses are close to linear relationships. Figure 8(a) shows the response of the eight sensor probes we have fabricated and they are all near linear. So, polynomial fits can be used to obtain the temperature information. Figure 8(b) shows the

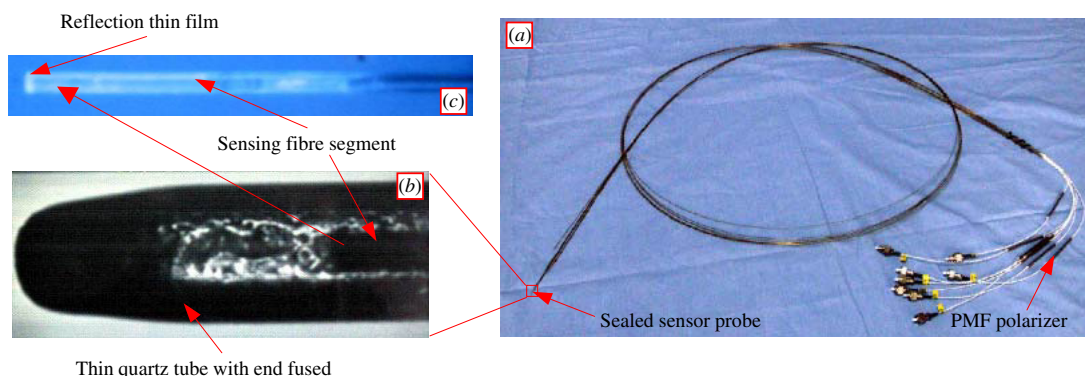


Figure 7. Sensor probe and packaging.

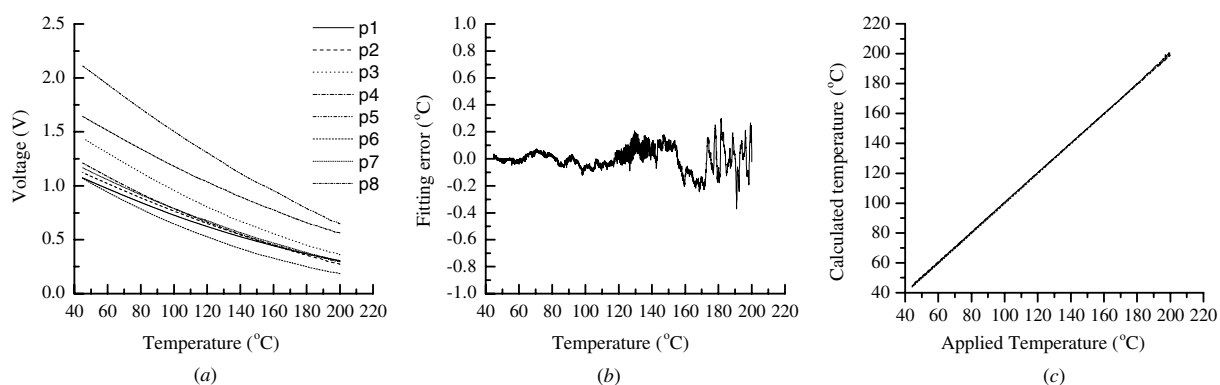


Figure 8. (a) Original output; (b) typical fitting error curve; (c) calculated temperature versus applied temperature.

typical temperature error for one of the sensors with a third-order polynomial fitting as the following equation:

$$T = b_0 + b_1x + b_2x^2 + b_3x^3 \quad (6)$$

where b_0 – b_3 are the model coefficients determined by calibration. The maximum error is $0.37\text{ }^\circ\text{C}$ within $+40\text{ }^\circ\text{C}$ – $+220\text{ }^\circ\text{C}$ temperature range. Figure 8(c) shows a typical curve of calculated (fitted to one curve in figure 8(a)) temperature values versus applied temperature. Good linear relationships have been obtained.

4.4. Prototype calibration and test results

The prototype was made, and a calibrated system, which consists of a precision oil bath, a standard thermometer and special software which is used to calculate the coefficients, was set up. The eight individual sensor probes have been calibrated with this system within the $-30\text{ }^\circ\text{C}$ to $240\text{ }^\circ\text{C}$ range, and the coefficients were calculated and embedded in the micro processor in the prototype. To investigate the accuracy of the prototype sensors, the test was done by the Changcheng Institute of Metrology and Measurement (CIMM) which has the first grade temperature measurement qualification in China and can make large range temperature measurements. The test temperature range is from $0\text{ }^\circ\text{C}$ to $200\text{ }^\circ\text{C}$. The test was done at 11 applied temperature points with about $20\text{ }^\circ\text{C}$ intervals. The typical measurement error is shown in figure 9 and the absolute errors of the eight sensors are all less than $0.5\text{ }^\circ\text{C}$. The test results show that the prototype has the required accuracy

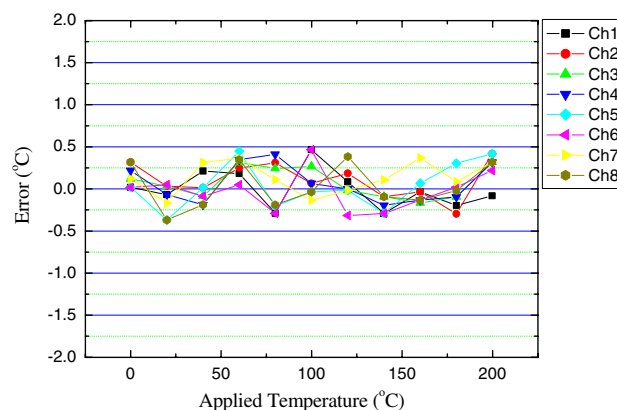


Figure 9. The test results.

and satisfies the demand for the field monitoring of power transformers.

5. Summary

A practical polarization maintaining optical fibre temperature sensor and relative technology for field hot-spot monitoring in power transformers were demonstrated. With special coating, packaging and processing technologies, prototype sensors were made and found to satisfy the demand of harsh environment and performance specifications required

by real time applications. The sensors have tiny sensor probes and high accuracy and can be used to perform accurate and safe temperature sensing on very small electro-explosive devices (EEDs) and process temperature monitoring in explosive or flammable material manufacturing or storage.

Acknowledgments

This work was supported by the Program for New Century Excellent Talents in Universities of China under grant no NECT-05-0183 and the National Natural Science Foundation of China under grant no 60207002. The authors would like to gratefully acknowledge the financial support provided by Shenyang Tianzhen Electric Transportation and Transformers Equipment Manufacture Co. Ltd.

References

- [1] Wang C and Mbi A 2006 *Meas. Sci. Technol.* **17** 1741–51
- [2] Alahbabi M N *et al* 2006 *Meas. Sci. Technol.* **17** 1082–90
- [3] Kuang K S C *et al* 2002 *Meas. Sci. Technol.* **13** 1523–34
- [4] Michie A *et al* 2005 *17th Optical Fibre Sensors Conf. Technical Digest (May)*
- [5] Bosselmann T *et al* 2005 *17th Optical Fibre Sensors Conf. Technical Digest (May)*
- [6] Bohnert K *et al* 2005 *17th Optical Fibre Sensors Conf. Technical Digest (May)*
- [7] Norton E T *et al* 1997 *Substation Equipment Diagnostics Conf.* vol 5 February
- [8] Yang Y 2004 *Chin. Opt. Lett.* **2** 259–61
- [9] Yang Y *et al* 2005 *17th Optical Fibre Sensors Conference Technical Digest, (May)*
- [10] Marrone M J and Davis M A 1985 *Electron. Lett.* **21** 703–4
- [11] Ourmazd A *et al* 1983 *Appl. Opt.* **22** 2374–9
- [12] Lefever H 1993 *The Fibre-Optic Gyroscope* (Boston, MA: Artech House) chapter 5